



Influence of Geo-stress on Dynamic Response Characteristics of Coal and Gas Outburst

Bin Zhou¹ · Jiang Xu¹ · Shoujian Peng¹ · Fazhi Yan¹ · Wei Yang² · Liang Cheng¹ · Guanhua Ni³

Received: 28 November 2019 / Accepted: 19 May 2020 / Published online: 13 June 2020
© Springer-Verlag GmbH Austria, part of Springer Nature 2020

Abstract

The influence of tectonic, geostatic, and mining stresses on coal and gas outburst (CGO) becomes more obvious with increasing mining depth. The limitations of general experimental methods and test systems hinder the direct observation and characterization of the dynamic responses of the multi-physical parameters associated with CGO. In this study, a custom-made large-scale physical simulation test system was used to study the characteristics of outburst evolution under different geo-stress levels, to overcome dynamic disasters in coal mines. The intensity and initial velocity of the outburst coal flow increased with increasing geo-stress. The geo-stress changes and gas pressure released during the outburst process mainly manifested in the relief and abutment stress zones, while the release of the elastic strain energy manifested in the abutment stress zone. This showed that the sphere of influence of the change on the physical parameters, such as the geo-stress, gas pressure, and elastic strain energy, is important for setting the drilling depth in measures to eliminate outburst. Interestingly, there seems to be a mechanism that suppresses the excess energy released during the outburst process, such that the solid–gas ratio of the two-phase outburst flow does not increase with increasing initial geo-stress. The dynamic outburst phenomenon is not completely positively correlated with increasing geo-stress. The mechanism causes cyclical fluctuations in the geo-stress, elastic strain energy, and gas pressure during the CGO process and pulse characteristics of the outburst coal flow simultaneously.

Keywords Outburst · Geo-stress · Gas pressure · Elastic strain energy · Dynamic disaster

1 Introduction

Worldwide coal production increased by 250 Mt in 2018, an increase of 3.3%. This growth can be significantly attributed to the 4.5% increase in coal production in China (International Energy Agency 2019). More than 90% of China's coal production comes from underground mining, with about 53% of the total coal resources located 1000 m or deeper (Xie et al. 2019). With the depletion of shallow coal resources in recent years, mining operations are progressing deeper at a rate in the range of 10–20 m (highest: 50 m) per year (Wang et al. 2018a, b, c). Coal mine disasters under high geo-stresses that followed have become increasingly serious, significantly restricting the efficient mining of coal. Among the disasters are coal and gas outbursts (CGO) (Singh 1984; Alexeev et al. 2004; Chen 2011; Dutka et al. 2013; Zhao et al. 2016; Sun et al. 2016; Wang et al. 2018a, b, c). CGO is a dynamic phenomenon characterized by a rapid release in the elastic strain energy and gas expansion energy in the coal body (Valliappan and Zhang 1999;

✉ Shoujian Peng
sjpeng@cqu.edu.cn

Bin Zhou
18234086637@163.com

Fazhi Yan
yfcumt@163.com

¹ State Key Laboratory of Coal Mine Disaster Dynamics and Control, Chongqing University, Chongqing 400030, China

² Key Laboratory of Coal Methane and Fire Control, Ministry of Education, China University of Mining and Technology, Xuzhou 221116, Jiangsu, China

³ College of Mining and Safety Engineering, Shandong University of Science and Technology, Qingdao 266590, China

Sobczyk 2011; Skoczylas et al. 2014; Wang et al. 2018a, b, c; An et al. 2019). A typical characteristic is the rapid migration of the two-phase coal–gas medium in the roadway. Significant casualties and equipment losses have been reported in a short period of time (Lama and Bodziony 1998; Aguado and Nicieza 2007). The mechanism of CGO, which is a multi-factor-coupled dynamic disaster, remains unclear; most results are based on empirical assumptions (Xue et al. 2014). It has been generally accepted that CGO is a result of the combined effect of geo-stress, gas pressure, and the inherent properties of coal (Wold et al 2008; Li et al. 2017).

The stress in a coal seam gradually increases with an increase in the burial depth, resulting in the deformation of the coal seam and a corresponding increase in the elastic strain energy (Xie et al. 2019). A parametric analysis through numerical simulations has shown that the risk of CGO increases with increasing burial depth (Xue et al. 2014). To explore the mechanism of CGO, Alexeev et al. (2004), Jasinge et al. (2011), Peng et al. (2015), Xie et al. (2017) and Liu et al. (2019) studied the mechanical properties and failure mechanism of a coal–rock mass by conducting conventional uniaxial/triaxial experiments. They provided a basis for studying the initiation mechanism of CGO and the mechanical evolution characteristics in the development stage. The tectonic stress and its influence on CGO has been gradually recognized in recent years. Studies have shown the formation of gas bags in the coal seam under the action of tectonic stress, often leading to a CGO (Li 2001; Tu et al. 2016). Jiang et al. (2011) investigated the relationship between magma intrusion and CGO in terms of petrographic chemistry, micropores, and adsorption characteristics of coal Cao et al. (2003).took chloroform extracts from coal samples under a geological structure as a predictor of CGO and concluded that structural deformation may change the hydrocarbon generation potential of coal.

Lu et al. (2017) designed a multi-functional physical simulation implementation system to conduct a physical simulation experiment on CGO under the action of deep high geo-stress and study coal–rock engineering problems in complex stress environments Cao et al. (2019). proposed a test system that can be used to apply axial (3000 t) and horizontal symmetric (2000 t) loads on 1.5 m × 0.8 m × 0.8 m specimens. Based on a CSIRO model, Li et al. (2018) proposed a large-scale true three-dimensional CGO simulation experiment system that can be used to apply true three-dimensional gradient loading on test models with dimensions of up to 1.5 m × 1.5 m × 3 m. To simulate the mining environment to a certain extent and facilitate the flexible design of geological models, Nie et al. (2015) developed a medium-scale physical simulation device for CGO. In the above research, although the CGO was reproduced to some extent, the influence of true triaxial multi-level stress on CGO was not studied. Moreover, because of the lack of

multi-parameter evolution data related to the CGO process, no in-depth analysis has been conducted on the mechanism of geo-stress in the CGO process.

In this work, a custom-made large-scale physical simulation test system was developed to conduct experiments on the characteristics of CGO evolution under different geo-stress levels, to provide a better understanding of the dynamic disaster mechanism in coal mines. We analyzed the fluid dynamic phenomena, evolution process of the geo-stress, release of the elastic strain energy, and variation in the gas pressure during the CGO process. Accordingly, we report the response characteristics of CGO under different geo-stress levels, including the tectonic stress, in this paper.

2 Experimental Section

2.1 Sample Collection Site

Shuijiang Coal Mine is located in the northeast of Nanchuan, Chongqing, China. The wellhead of the main adit is located at 29° 11' 15"N and 107° 16' 52"E (Fig. 1). Currently, the only exploitable K 1 coal seam is 1082 m deep; the absolute gas emission is 9.83 m³/min, and the relative gas emission is 48.75 m³/t. According to incomplete statistics, since the first CGO (December 30, 1984), more than 110 CGOs have been recorded. The initial CGO depth was 264 m, the maximum CGO intensity was 1050 t, and the maximum CGO gas emission was 10⁵ m³.

The mining area is a boat-like syncline structure with compact folds and many faults, which have a destructive effect on the coal seam. The geological structure in the region was formed by the strong folds and fractures of the Yanshan movement during the Cretaceous. The complex fold structure significantly increases the risk of CGO in the mine. The Longtan Formation of the Upper Permian is a coal-bearing stratum, containing one layer of coal, namely the K 1 coal seam. The coal seam structure is complicated, and the main mining section is 0.7–3.2 m thick with an average thickness of 1.83 m. Figure 1 shows the thickness of the formation and the characteristics of the coal seam.

Table 1 lists the basic parameters of the coal samples collected from the mine. The coal samples were prepared according to the test methods given by Su (2014) and Zhang et al. (2018) as the coal briquette for the test. Table 2 lists the detailed proportions.

2.2 Experimental System

To study the dynamic response characteristics of CGO under different geo-stress levels, a custom-made multi-field coupled large-scale physical simulation test system (Fig. 2) was used to conduct experiments. The system can

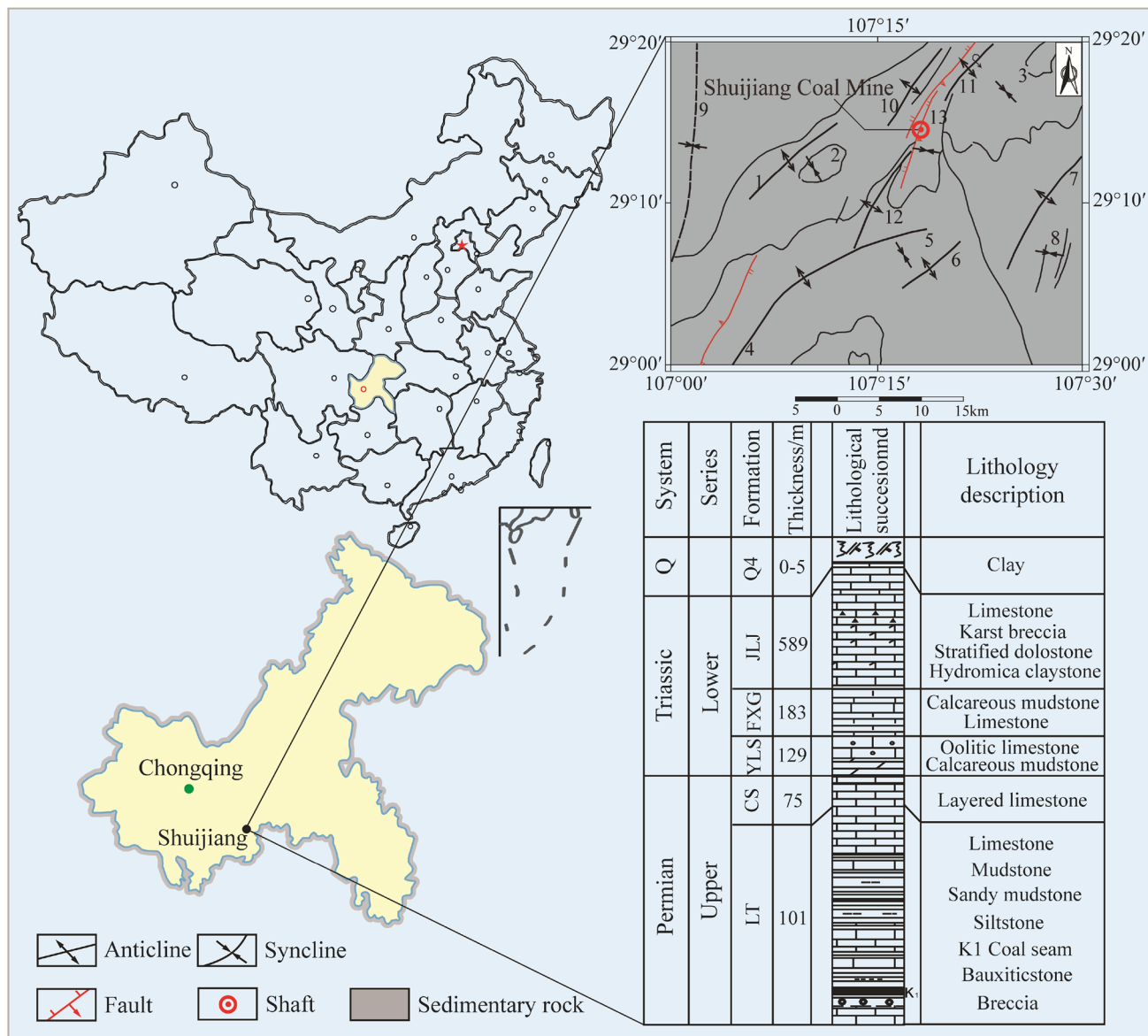


Fig. 1 Petrographic and geochemical characteristics of study site

Table 1 Basic parameters of the coal sample

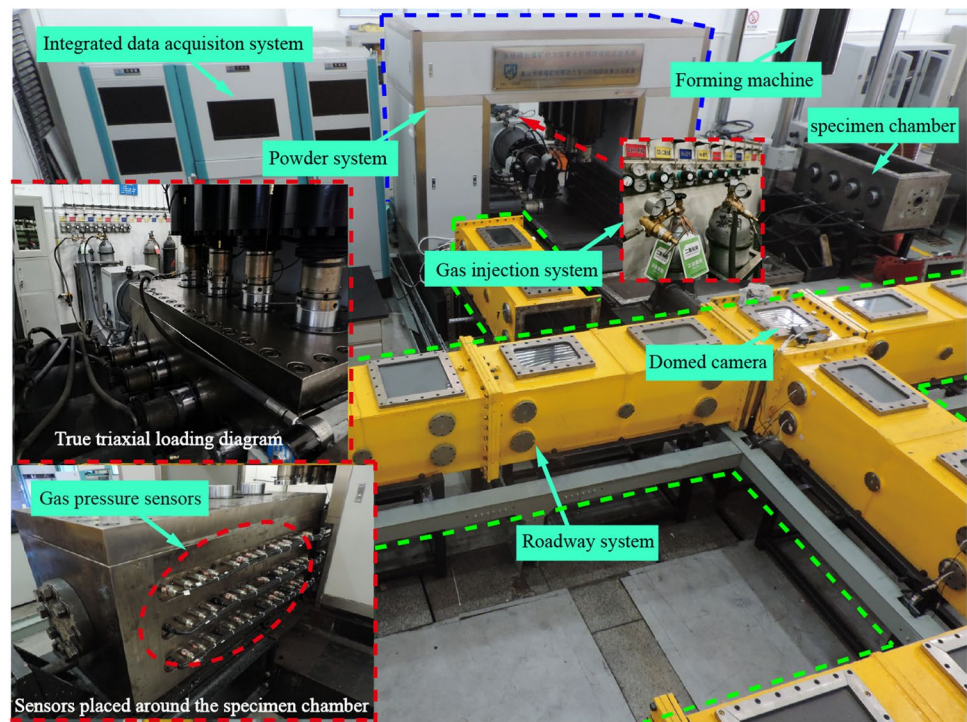
Coal seam	Proximate analyses (%)				Adsorption constant		Sulfur content (%)	True density (t/m ³)	ΔP (mm Hg)	Firmness coefficient
	Mois	Ash	VM	PC	a	b				
K 1	0.30	23.94	12.90	62.86	12.4	1.66	4.58	1.45	6.00	0.59

Mois moisture, VM volatile component, PC fixed carbon, ΔP initial discharge velocity of coalbed methane

Table 2 Briquette particle size distribution

Particle size (mm)	<0.150	0.150–0.180	0.180–0.250	0.250–0.425	Polyvinyl acetate adhesive	Gypsum	Water
Mass percentage (%)	50.5	5.8	11.6	22.3	6.8	3	4

Fig. 2 Large-scale test system for the physical simulation of dynamic disasters in coal mines

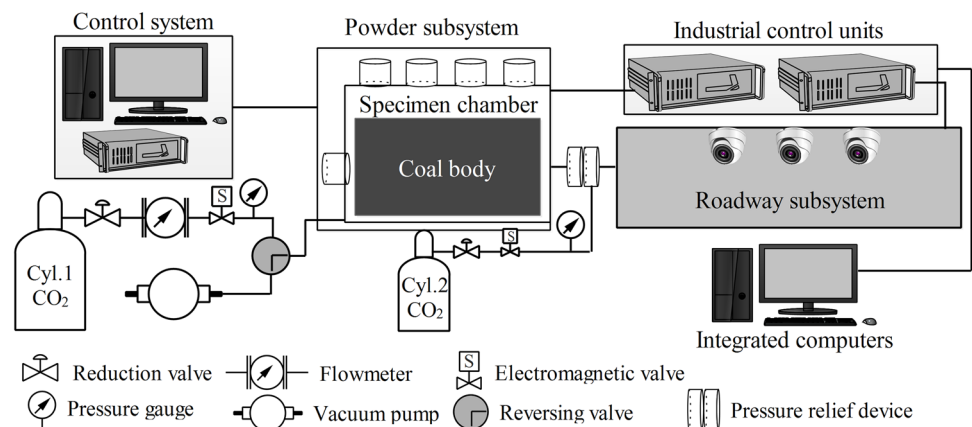


reflect the true triaxial stress state of the coal body in the process of CGO under the action of gas–solid coupling. In addition, the two-phase CGO flow enters the roadway system, thus providing a more accurate simulation of the dynamic process occurring in the coal mine. The core components of the experimental system include a power subsystem and a roadway subsystem. The power system is the device generating the CGO. The specimen chamber along with the true triaxial loading device can reproduce the stress state of a coal body with a size of 400 mm × 400 mm × 1050 mm. Through multiple sets of hemispherical cameras placed in the roadway, the motion characteristics of the coal powder during CGO can be observed. Based on this system, we can simultaneously

determine the variations in the geo-stress and gas pressure in the coal body during the CGO process.

A schematic for the experiment setup, as shown in Fig. 3. The vacuum pump is used to ensure the purity of the CGO gas during the experiments. The gas cylinder 1 (Cyl. 1) provides CGO gas into the specimen chamber. The electromagnetic valve and pressure gauge are used to achieve equal gradient injection of gas pressure until it reaches a predetermined gas pressure value of 1.5 MPa. The gas cylinder 2 (Cyl. 2) provides gas to the pressure relief device to adjust the pressure difference between the specimen chamber and the roadway. In this way, accurate control of gas pressure in the coal body is achieved. The roadway subsystem is directly connected to the specimen chamber through the

Fig. 3 Schematic of the physical simulation test system



pressure relief device. The control system is used to load the geo-stress to the coal body. The two sets of industrial control units collect the geo-stress, gas pressure, and image information while transmitting them to an integrated computer.

2.3 Experimental Scheme

The influence of tectonic, geostatic, and mining stresses on CGO is mainly reflected in the stress level and direction. In common engineering measures, the purpose of reducing the risk of coal mine dynamic disasters is achieved by removing the stress values (Zhou et al. 2018; Aguado and González 2009). As such, the experiments focus on the effects of different stress levels on CGO. The stress state of a coal body in front of the work face of a deep coal mine starts from a quasi-hydrostatic pressure state. With the advancement of the working face, the vertical stress increases from a three-way isobaric state to the abutment stress zone and then enters the relief stress zone (Xie et al. 2019). When the ratio of the maximum horizontal principal stress to the minimum horizontal principal stress is 0.6, the similarity ratio of geo-stress is 12.0, and the gas pressure ratio is 1.0 (Cai 2002; Zhang et al. 2016; Zhao et al. 2018). Figure 4 shows

the stress loading mode during the test. It should be noted that the stress loading of the four zones of the coal body in our experiments was presented in a “jumping” manner. After buffering in the recovered stress zone, the slope of stress increasing in the vertical direction for different experiments were 3.8 MPa/m, 7.7 MPa/m and 15.3 MPa/m, respectively. The slope of stress increasing in the horizontal direction for different experiments were 2.3 MPa/m, 4.6 MPa/m and 9.2 MPa/m, respectively. Table 3 lists the stress values in each direction.

A total of nine stress measuring points are located inside the loading head during the experiment, and a total of 36 gas pressure measuring points are distributed concentrically in different areas of the coal body. The following were the main steps involved in the experimental process:

Sample preparation and Sensor arrangement: After the raw coal was crushed, it was cold-formed under a pressure of 12 MPa according to the mass ratio listed in Table 2. It needs to be illustrated that in consideration of the reconstructed coal has many advantages in experimental study especially its homogeneous structure and excellent repeatability, so the coal briquette coals were used in this

Fig. 4 Stress state of specimen and arrangement of gas pressure sensors

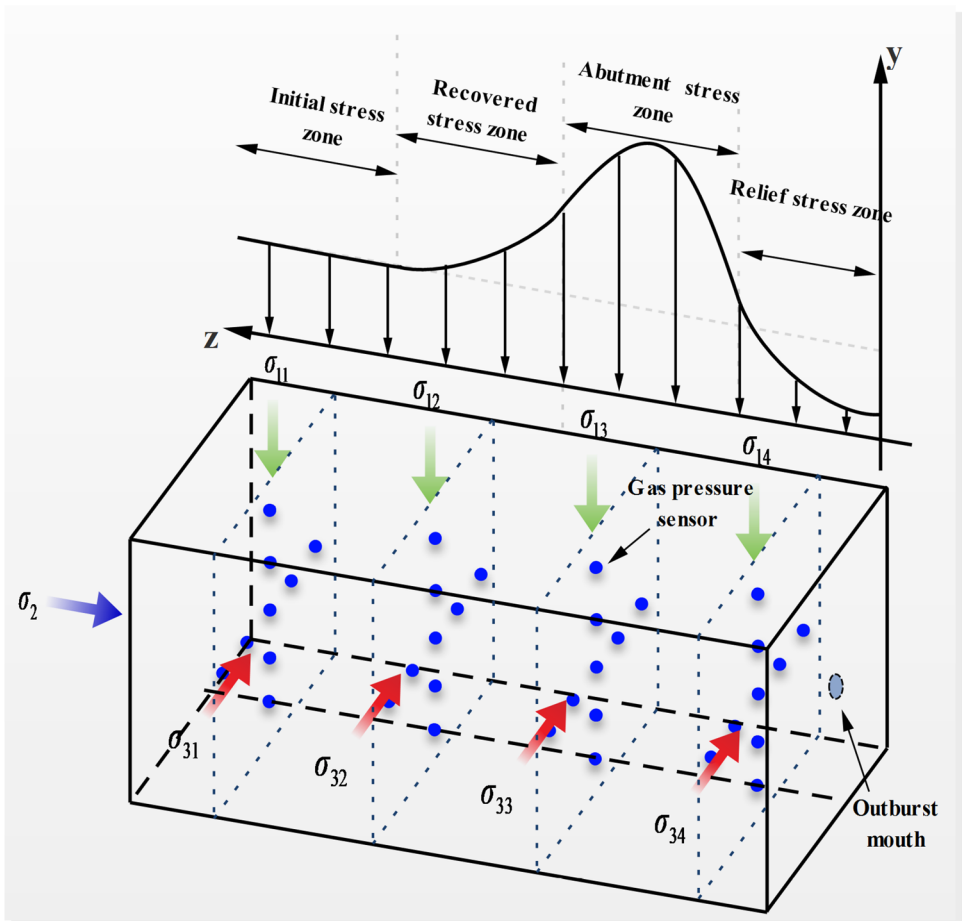


Table 3 Geo-stress and gas pressure scheme

	Gas pressure (MPa)		Geo-stress (MPa)							
			Vertical stress				Horizontal stress 1#			
	σ_{11}	σ_{12}	σ_{13}	σ_{14}	σ_{31}	σ_{32}	σ_{33}	σ_{34}	σ_2	
1.5	1.0	1.5	2.0	0.5	0.6	0.9	1.2	0.3	1.0	
	2.0	3.0	4.0	1.0	1.2	1.8	2.4	0.6	2.0	
	4.0	6.0	8.0	2.0	2.4	3.6	4.8	1.2	4.0	

Table 4 Outburst coal mass and RIO characteristics

Geo-stress (MPa)	Specimen mass (kg)	Ejected coal (kg)	RIO (%)
1.0	223.55	14.20	6.35
2.0	211.30	16.84	7.97
4.0	223.70	20.01	8.95

study. During the process of loading the coal sample into the specimen chamber in batches, the gas pressure sensor is buried, as shown in Fig. 4. After the coal sample is formed in five times, the specimen is sealed.

Vacuum treatment: After sealing the specimen chamber, a vacuum treatment is performed for 4 h, so that the pressure inside the chamber is reduced to -0.1 MPa, thus ensuring that the inside of the chamber is in a vacuum environment.

Inflatable adsorption: The experimental gas (CO_2 was used as CGO gas during the experiments) is injected into the specimen chamber in stages until the gas pressure stabilized at 1.5 MPa.

Geo-stress loading: The geo-stress was applied in stages to the values, listed in Table 3, and stabilized for 1 h.

CGO trigger: The multi-stage pressure relief device is adjusted to induce CGO and simultaneously trigger the data acquisition system.

3 Results

3.1 Intensity of CGO

The most direct manifestation of CGO is the motion of the coal and gas in the roadway. While quantitatively measuring the destructiveness of CGO, the mass of the coal entering the roadway after CGO is generally used. Taking into account the possible differences in the initial coal loading mass during each experiment, the relative intensity of CGO (RIO) is used as an indicator to evaluate the destructiveness of CGO, which is defined as the ratio of the mass of coal entering the roadway to that of the initial specimen (Geng et al. 2017; Jin et al. 2018). Table 4 lists the total mass values

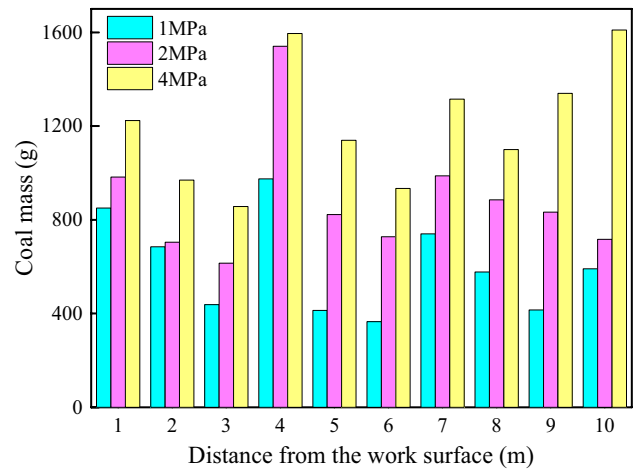


Fig. 5 Accumulation characteristics of coal within 10 m from the working face

of the specimens and CGO intensity at different geo-stress levels. As the geo-stress increases, the RIO increases significantly, but not proportionally with the geo-stress. Reducing the initial geo-stress in the coal seam is feasible for reducing the intensity of CGO. In addition, the working face is divided into 10 zones up to a range of 10 m, and the coal mass distribution in each zone is determined, as shown in Fig. 5. The increase in the CGO intensity is reflected in each zone, i.e., as the initial geo-stress increases, the mass of the coal in each zone increases within 10 m from the front of the working face. The mass accumulation characteristics of the coal can directly reflect the energy consumption in the dynamic process, i.e., the work required to carry the coal powder. However, the scope of this research is limited to the mechanism of CGO.

3.2 Visual Representation of CGO

The visual characteristic of the CGO phenomenon is that under the action of gas drag force, the coal particles move at a high speed in the roadway. It is difficult to directly obtain a morphological representation of CGO and perform an experimental simulation because of the rapid flow and expansion of the gas, the impact of high-speed coal particles, and the

complex wave system in the roadway. We recorded the entire CGO process under different geo-stress levels using a domed camera. Figure 6 shows single-frame images captured soon after the CGOs were triggered. At 0.60 s, the volume fraction of the coal particles ejected in the roadway is relatively low, and only fine coal particles are present at the bottom of the roadway. Comparing the frontier contours of the pulverized coal under the different geo-stresses at this moment, we find that the frontier of the pulverized coal expands more widely with an increase in the initial geo-stress of the coal seam. This indicates that the initial velocity of the coal increases with increasing geo-stress. From this, we can conclude that the impact at the onset of CGO is enhanced under high geo-stresses.

When the CGO lasted for 1.00 s, the volume fraction of the pulverized coal increased. Comparing the results obtained under different geo-stress conditions, we find that the volume fraction of the pulverized coal increases the most when the geo-stress is increased from 1 to 2 MPa. However, when the geo-stress is increased from 2 to 4 MPa, the volume fraction is significantly reduced. This unexpected result indicates that the dynamic phenomenon of CGO is not completely positively correlated with increasing geo-stress. In other words, there is a point at which the trend in the geo-stress value reverses. When the initial stress in the coal seam reaches this point, CGO is no longer enhanced. In the extreme case, the geo-stress increases indefinitely, and the flow velocity and solid–gas ratio of the two-phase gas–coal medium are unlikely to continue increasing. The cross-sectional area of the hole and roadway will also limit the dynamic characteristics of the two-phase gas–solid medium. More details are

provided in the discussion section. At 2.0 s, the coal under a geo-stress of 1.0 MPa begins to subside, whereas the CGO processes under geo-stress levels of 2.0 and 4.0 MPa continue. This indicates that the flow time is less when the geo-stress is low.

The most intuitive dynamic parameter of the coal is the motion speed. Zhao et al. (2017) found the flow speed of outburst coal from Zhongliangshan field to be 12.2 m/s, which is one of the highest values calculated from field data. The maximum speeds of outburst coal obtained by Jin et al. (2018) and Sun et al. (2018) were 41.02 and 16.82 m/s, respectively. The calculation method of the pulverized coal speed during the CGO experiment usually depends on the position of the frontier contour of the pulverized coal in the image of a certain frame and the corresponding shooting time. Undoubtedly, when the shooting frame rate during the experiment is insufficient or when the focusing effect is not ideal, it is difficult to calculate the pulverized coal speed, and some interesting phenomena of the two-phase flow in the CGO process will be lost. Since a black coal powder corresponds to a gray value of 0, for a group of cameras, the closer the pulverized coal is to the camera position, the lower the gray value of the captured image. Therefore, directly explaining the motion characteristics of outburst coal using the gray value of the image of each frame can help avoid the above problems, with convincing results.

Figure 7 shows the variations in the gray value of the acquired images during the three CGO experiments. The variations in the gray-scale value is defined as the difference between the gray-scale value of the digital image during the CGO process and the gray-scale value at the start of the CGO. It is calculated as follows:

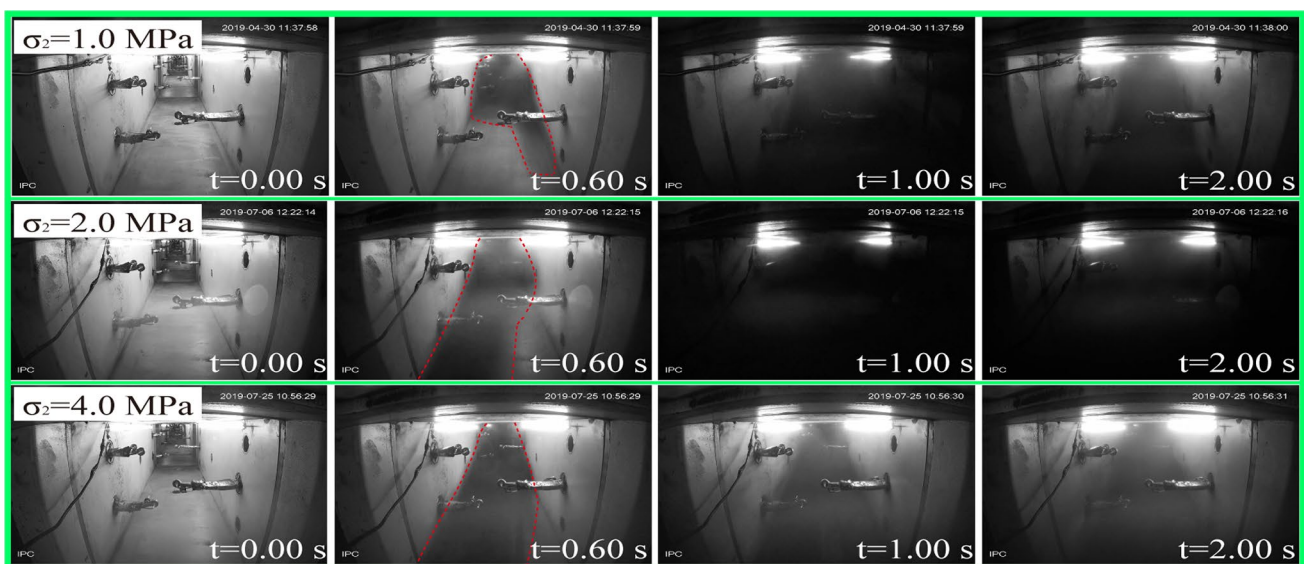


Fig. 6 Images of the coal outburst during CGO

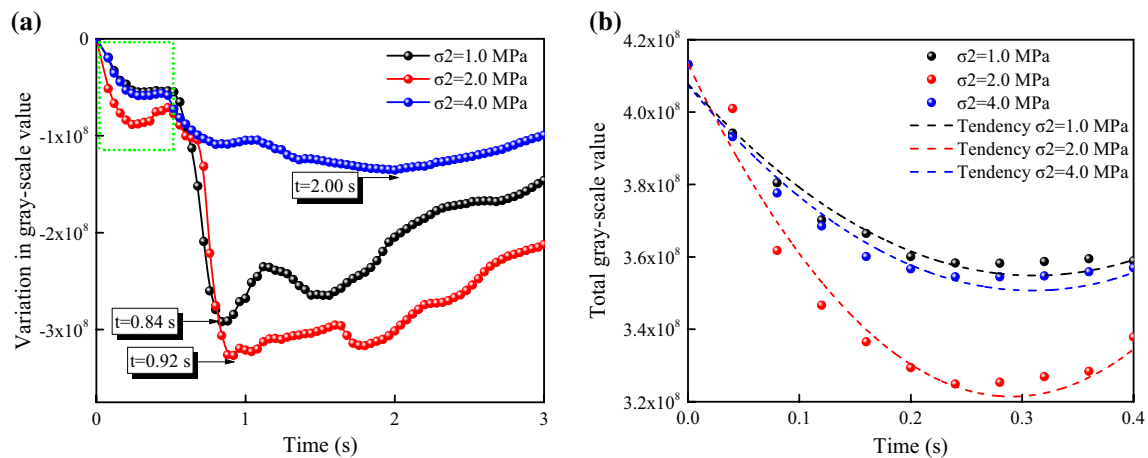


Fig. 7 Variation in the gray-scale value of images taken during coal outburst

$$V_{\text{gray}} = G_{\text{gray}i} - G_{\text{gray}0},$$

where V_{gray} represents the variations in the gray-scale value; $G_{\text{gray}i}$ represents the gray-scale value corresponding to the i -th image; and $G_{\text{gray}0}$ represents the gray-scale value corresponding to the first image (that is, the start time of CGO).

Figure 7a shows that when the CGO lasts for 0.84 s, the volume fraction of the coal particle is the highest under a geo-stress of 1 MPa, and the gray value is the lowest. As the geo-stress is increased to 2.0 and 4.0 MPa, the gray values are lowest at 0.92 and 2.00 s, respectively. Therefore, as the geo-stress increases, the solid–gas ratio of the coal–gas flow after CGO becomes maximum much later. Unexpectedly, the higher the geo-stress, the greater the elastic strain energy stored in the coal. This should have led to more pulverized coal. However, when the geo-stress reaches 4.0 MPa, the gray value associated with the CGO process is significantly reduced. This suggests that there is a mechanism that suppresses the excess energy released during the dynamic process. Furthermore, the gray-scale value is not instantaneously minimized; it is characterized by multiple undulations, which indicate intermittent characteristics of the CGO process. Figure 7b shows the gray value information of the image captured when the CGO lasts for 0.4 s. After the CGO is activated, the coal powder is thrown instantaneously, and the gray value of the image is reduced. At about 0.3 s, the gray value starts to increase, indicating a decrease in the volume fraction of the coal particles in the roadway. Subsequently, as shown in Fig. 7a, after a brief recovery, the gray value once again decreases. This intermittent characteristic of CGO is related to the choking phenomenon of the two-phase flow in the CGO cavern and the roadway (Jaworski and Dyakowski 2002; Chen 2011).

3.3 Geo-stress Characteristics of CGO

The effect of geo-stress on CGO is reflected in the elastic strain energy reserve in the CGO preparation stage and in the continuous failure of the coal body in the development stage. Once the outburst is triggered, the coal body in the relief stress zone is instantaneously transformed into a two-direction force state. Accompanying phenomena include the flow and desorption of the gas because of the differences in the pressure gradients in the coal seam and roadway. These represent the “coal–gas–surrounding rock–roadway” system, which voluntarily transitions from an unbalanced state to another equilibrium state, i.e., stress transfer takes place to eliminate the imbalance.

Figure 8 shows the evolution process of the geo-stress in the different parts of the coal seam during the CGO process. The changes in the geo-stress during the CGO process are mainly manifested in the relief stress zone and the abutment stress zone, whereas the geo-stress in the recovered stress zone and initial stress zone fluctuates only slightly in the CGO process. In the relief stress zone, the horizontal stress decreases faster than the vertical stress during the CGO process. When the CGO lasts for 0.96 s, the horizontal stress (4 MPa) is reduced to the lowest point (0.18 MPa), while the stress in the vertical direction is still in the descending stage. Once the stress value drops to the lowest point, it will increase again. This indicates that even if caverns or multiple cracks are formed during the CGO process, the coal body in the zone will have a certain supporting capacity. When the stress value increases beyond the strength of the coal body, it will be unloaded again. Figure 8a, e show the fluctuations in the stress drop process. The geo-stress change in the abutment stress zone lags behind that in the relief stress zone, indicating that CGO is a dynamic

process from the beginning of the relief stress zone to the deep transfer of the coal body. Similarly, the abutment stress zone also exhibits periodic fluctuations during the unloading process. In the recovered stress zone, the geo-stress value does not decrease during the CGO process; a small increase is observed (Fig. 8c, g). This phenomenon is particularly obvious under a geo-stress of 4.0 MPa. This is consistent with the results obtained by Yin et al. (2015) and Xie et al. (2019) in that the geo-stress concentration in front of the work face will gradually move deeper into the coal seam after CGO. During the three CGO tests, the geo-stress in the initial stress zone remains the same.

Comparing the three experiments, we noticed that when the initial geo-stress of the coal seam is 1.0 MPa, the stress fluctuates during the CGO process, but after 4 s, the stress in each zone returns to the original state. Notably, the phenomenon still exists when the initial stress of the coal seam is 2.0 MPa, but the vertical stress decreases before and after the occurrence of CGO (Fig. 8e, f). When the initial geo-stress of the coal seam increases to 4.0 MPa, the stresses in both the relief stress zone and abutment stress zone are significantly decreased. For example, the horizontal stress in the relief stress zone is reduced from 1.2 to 0.44 MPa, and the vertical stress is reduced from 2 to 0.42 MPa. This can be attributed to the difference between the coal bearing capacity and the geo-stress response. During the CGO process, the geo-stress increases, and it is easier to reach the destructive strength of the coal body, which in turn produces more coal particles. However, this does not mean that there is an obvious kinetic phenomenon in the roadway, because from a certain point of view, the amount of fluid medium increases, and it is more prone to clogging during the flow (Jaworski and Dyakowski 2002; Chen 2011; Zhou et al. 2019).

3.4 Evolution Characteristics of Elastic Strain Energy

Although the occurrence of CGO is affected by many factors, its main energy sources are the geo-stress and gas pressure. The influence of gas pressure on CGO is clear: the CGO intensity tends to increase with the increase in the gas pressure (Wang et al. 2018a, b, c; An et al. 2019). Based on the mass of outburst coal in the roadway, Valliappan and Zhang (1999) found that the gas expansion energy in the process of CGO is much greater than the elastic strain energy of the coal body. On this basis, Wang et al. (2018a, b, c) concluded that the contribution of gas pressure during a CGO is hundreds of times that of the geo-stress. Jin et al. (2018) and Sun et al. (2018) ignored the influence of geo-stress during the physical simulation experiment. Under the single factor, the influence of gas pressure on CGO was investigated, making the research target clearer. However, there are drawbacks in employing the mass of the coal in

the roadway as an indicator for calculating the energy source of CGO, because the elastic strain energy is not directly involved in the handling of coal particles as in the case of the gas expansion energy. Nevertheless, the strain energy directly affects the coal body fracture during CGO, which is directly related to the flow and impact dynamic characteristics of the two-phase gas–solid medium. To this end, we discuss the evolution of the elastic strain energy during CGO, which has rarely been done. Figure 9 shows the evolution of the elastic strain energy under three different experimental conditions. The elastic strain energy is calculated as follows (Huang and Li 2014; Hashemi and Melkoumian 2016):

$$W_e = \frac{1}{2E} [\sigma_1^2 + \sigma_2^2 + \sigma_3^2 - 2\mu(\sigma_1\sigma_2 + \sigma_1\sigma_3 + \sigma_2\sigma_3)], \quad (1)$$

where σ_1 , σ_2 , and σ_3 represent the geo-stresses in the three directions; μ represents the Poisson's ratio of the experimental specimen, $\mu = 0.158$ in the study; and E represents the unloading modulus of the experimental specimen, $E = 292$ MPa in the study.

The release of the elastic strain energy during CGO is manifested in the abutment stress zone. Its evolution process is similar to the change process of the geo-stress, and there are periodic cycle characteristics, indicating that the strain energy is not instantly released during the CGO process. This release characteristic is also an important factor for the pulsing phenomenon of CGO. When the initial geo-stress of the coal seam increases, the stored strain energy increases. Therefore, in the first energy release cycle, the energy release time under the 4.0 MPa test condition is the longest, reaching 1.44 s. Thereafter, the time of energy release and the number of cycles seem to be irregular. Based on the above results, the stress relief of the coal seam should be carried out around the abutment stress zone, so that the energy release of the geo-stress during the CGO process can be more effectively reduced.

Figure 10 shows the cumulative amount of the strain energy in each cycle of the abutment stress zone during the CGO process. When the geo-stress is 1.0 MPa, the elastic strain energy decreases from 8.00×10^{-3} to 5.75×10^{-3} J mm⁻³ and then starts to increase. At 4 s, the strain energy reaches 7.34×10^{-3} J mm⁻³. The strain energy decreased by 8.25% during the entire process. For a geo-stress of 2.0 MPa, the strain energy stored in the coal seam is 32.00×10^{-3} J mm⁻³. After two cycles of decline, it reduces to 11.90×10^{-3} J mm⁻³ and then begins to increase. Moreover, at 4 s, the strain energy is 19.61×10^{-3} J mm⁻³, and the strain energy change rate during the CGO process is 38.72%. In comparison, the strain energy at a geo-stress of 4.0 MPa is reduced from the initial value of 128.00×10^{-3} J mm⁻³ to the lowest value of 26.91×10^{-3} J mm⁻³ and finally reaches 31.89×10^{-3} J mm⁻³ after a slight rebound; the strain energy change rate is as high as 75.09%. Obviously, the increase

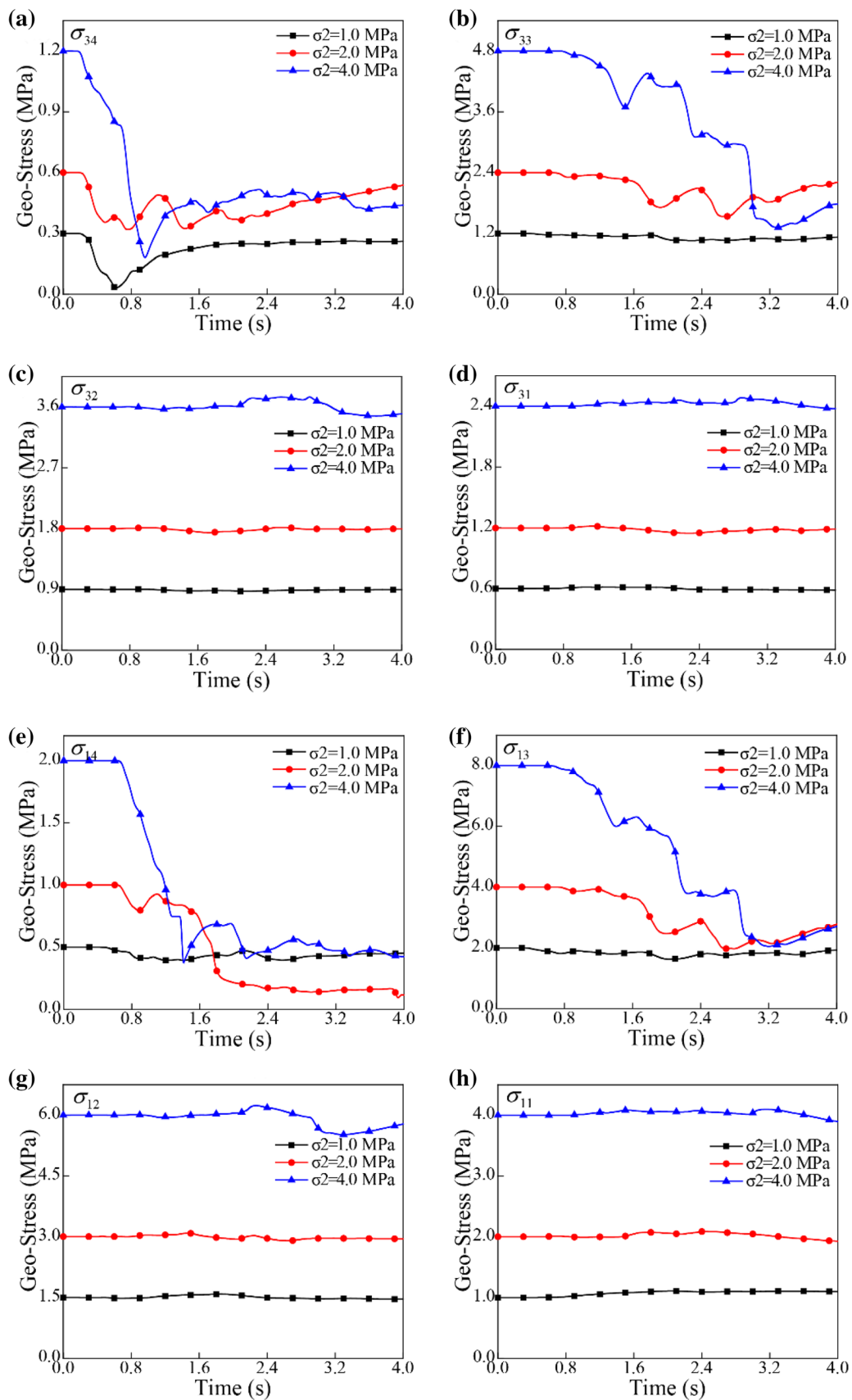


Fig. 8 Geo-stress evolution in different zones: **a** relief stress zone (σ_{34}), **b** abutment stress zone (σ_{33}), **c** recovered stress zone (σ_{32}), and **d** initial stress zone (σ_{31}) in the horizontal direction; **e** relief stress zone (σ_{14}), **f** abutment stress zone (σ_{13}), **g** recovered stress zone (σ_{12}), and **h** initial stress zone (σ_{11}) in the vertical direction

rate of the geo-stress is far less than the increase rate of the elastic strain energy released during the CGO process. When the initial stress of the coal seam is increased by four times from 1 MPa, the elastic strain energy released increases by more than nine times. From this point of view, when the burial depth of the coal seam is high and the structural stress increases sharply, the elastic strain energy can no longer be ignored, and the influence of the geo-stress on CGO should be equally emphasized.

3.5 Gas Pressure Characteristics of CGO.

Studying the critical gas pressure of CGO is an important research direction for predicting the dynamic phenomena (Skoczylas and Wierzbicki 2014). Currently, the critical gas pressures determined in China, Russia, and Czech are 0.74, 1.0, and 0.15 MPa, respectively (Ding and Yue 2018). However, even if the gas pressure is below the critical value, CGO can often occur. The geological conditions of the coal seam, the mechanical properties of the coal body, and the mining technology are different in each mining area. Exploring the characteristics of the gas pressure change during CGO is crucial for understanding the gas mechanism in the CGO process and rationally determining the critical gas pressure under multi-factor levels.

The gas evolution characteristics at the central position of each section of the coal seam in the different zones of CGO were selected for observation (Fig. 11). During the process of CGO, the decreasing gas pressure in the relief and abutment stress zones fluctuates; this is more obvious in the relief stress zone. However, the gas pressure in the recovered stress zone and initial stress zone appears to continue to decrease. After the CGOs were triggered, the gas rapidly expands through the CGO cavern and enters the roadway; its flow velocity does not continue to increase. According to the classical fluid mechanics theory, the flow rate of gas in the process of flowing from the coal seam to the roadway must satisfy the following relationship:

$$\frac{c^2}{\gamma - 1} + \frac{u^2}{2} = \text{Constant}, \quad (2)$$

where c represents the speed of sound; u represents the speed of the CGO gas; and γ represents the specific heat ratio.

Therefore, the maximum speed that the outburst gas can reach during the flow is the local speed of sound. When the maximum speed is reached, the gas pressure after the sound velocity section will no longer change. However, the gas in the coal seam will continue to desorb, causing the gas pressure to rise again. This is why the gas pressure in the relief and abutment stress zones fluctuates. Moreover, as the gas flows into the roadway, the CGO cavern acts as a link where negative pressure disturbances are generated to form multiple expansion and compression waves (Shapiro 1953; Qian 1966; Shankar and Deshpande 2003). During the deep propagation of the wave system to the coal seam, the direction of the CGO gas flow is opposite to the wave propagation, resulting in a slight increase in the gas pressure. In the recovered and initial stress zones, the decrease in the gas pressure during the CGO process is similar to that observed in a conventional desorption process.

In the experiments, the three different geo-stress conditions showed different gas pressure drop processes. As the geo-stress increases, the pressure drop curve shows more pronounced fluctuation characteristics (Fig. 11a, b). When the geo-stress is 1.0 MPa, choking occurs twice in the pressure drop process in the relief stress zone (C1 and C2 in Fig. 11a); this is not observed in the abutment stress zone. As the geo-stress increases to 2.0 MPa, there is a fluctuation in the abutment stress zone (C1 in Fig. 11b). When the initial geo-stress of the coal seam is 4.0 MPa, there are three obvious choking phenomena in the relief stress zone (C1, C2 and C3 in Fig. 11a), and the abutment stress zone also has two obvious fluctuations (C1 and C2 in Fig. 11b). The choking observed in the pressure drop process is directly related to the changes in the geo-stress during the CGO process. On the other hand, when the geo-stress increases, the gas pressure increases correspondingly, resulting in higher expansion energy and elastic strain energy. During the process of energy release, the outburst gas is more likely to reach the critical speed of sound, resulting in more obvious choking.

In addition, it can be seen from Fig. 11c, d that in the recovered stress zone and the initial stress zone, as the geo-stress increases, the rate of gas pressure change during CGO obviously increases. It is because the coal body in these zones have not been damaged during the CGO process, and the larger stress will cause greater deformation of the coal body. The direct consequence is that the pore pressure increases, resulting in a higher pressure gradient between the coal seam and the roadway.

To further investigate the spatial difference in the gas pressure changes in the coal seam during CGO, the gas pressure data obtained from 36 test locations were processed using a spline interpolation method (Sandwell 1987) to estimate the gas pressure change at other positions in the coal seam. Figure 12 shows the obtained gas pressure nephogram at different times during the test. During the process

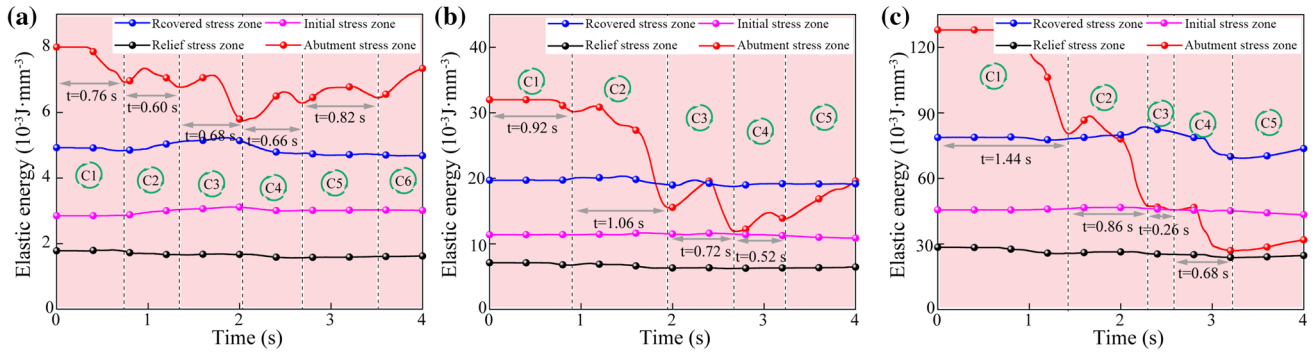


Fig. 9 Elastic energy in different zones: **a** Elastic energy at 1.0 MPa, **b** Elastic energy at 2.0 MPa, **c** Elastic energy at 4.0 MPa

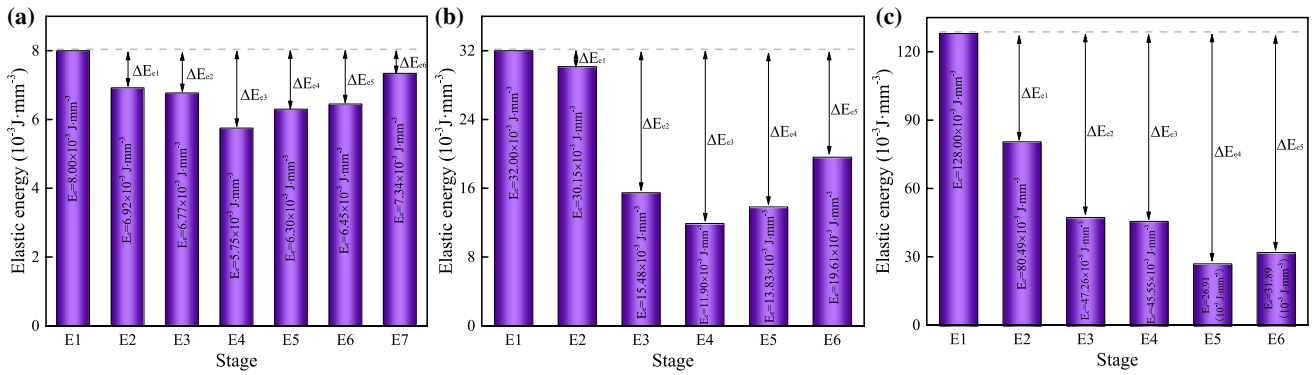
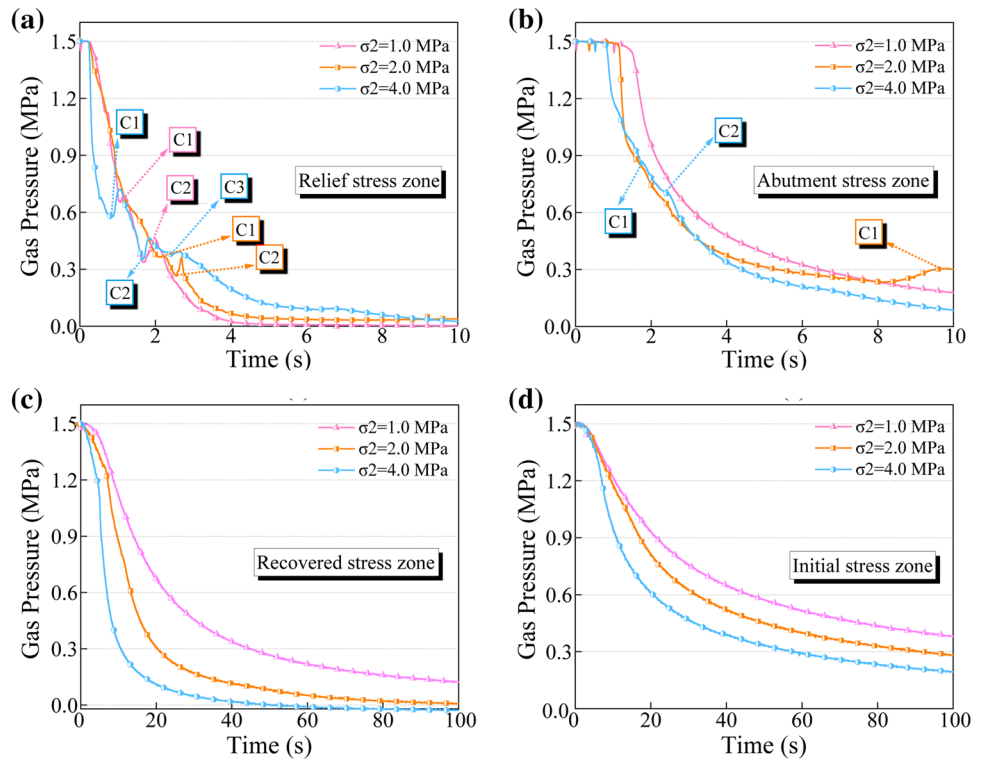


Fig. 10 Cumulative amount of strain energy in each cycle of the abutment stress zone: **a** Initial stress is 1.0 MPa, **b** Initial stress is 2.0 MPa, **c** Initial stress is 4.0 MPa

Fig. 11 Gas pressure of coal seam



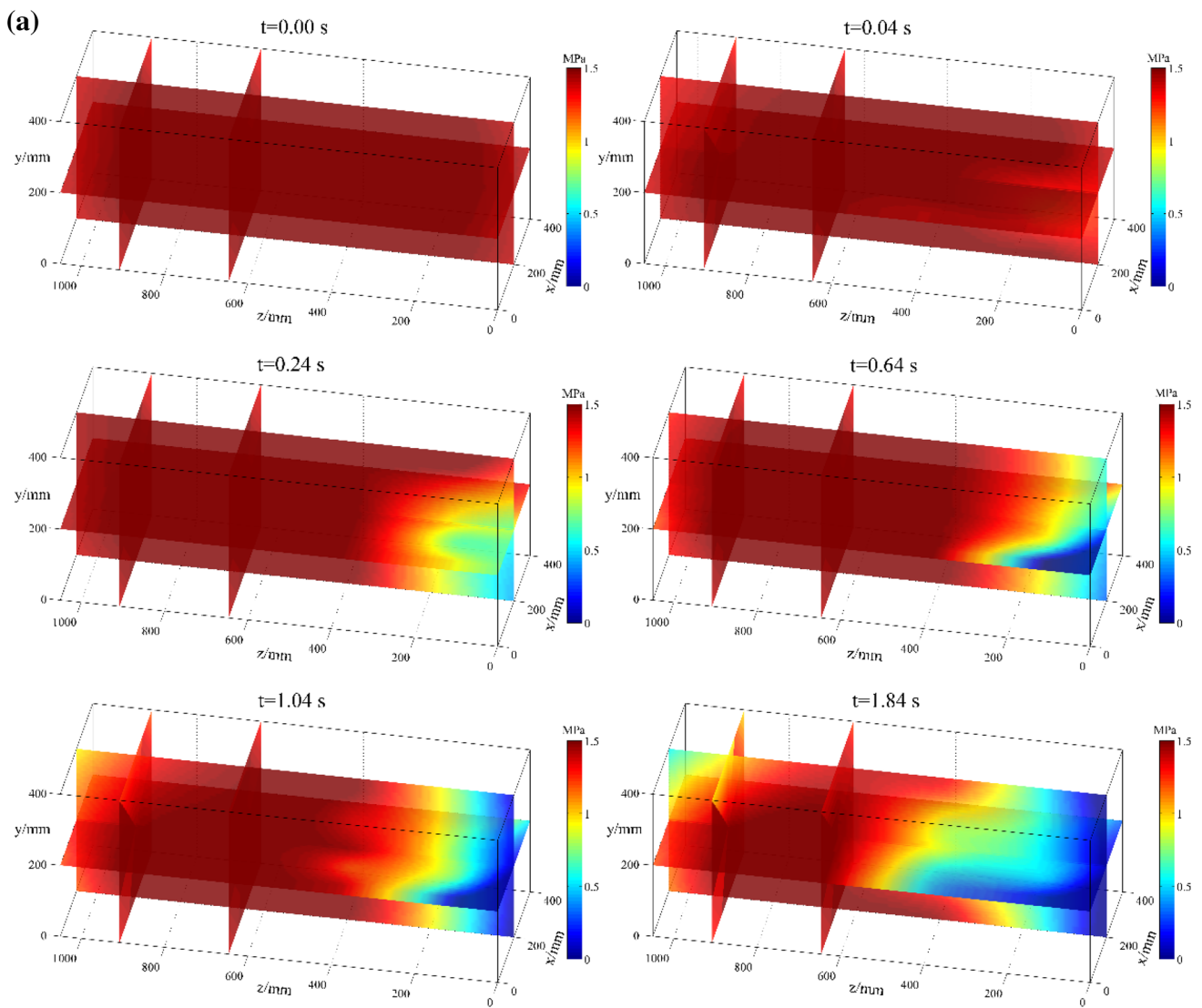


Fig. 12 Variations in the gas pressure of the coal seam under varying initial stress: **a** Initial stress is 1.0 MPa, **b** Initial stress is 2.0 MPa, **c** Initial stress is 4.0 MPa

of CGO, the pressure drop begins from the working face and gradually develops into the deep coal seam. Due to the difference in the principal stresses in the horizontal and vertical directions, the gas change in the coal seam does not exhibit a symmetrical structure. For real coal seams, in addition to the difference in the stress, the complex internal fissures and the heterogeneity of the coal structure make the pressure drop pattern more complicated. During CGO, the gas pressure is largely released in the relief and abutment stress zones. If we can determine the extent of this change in the gas pressure during the process, it will aid in setting the drilling depth in measures to eliminate CGO, such as advanced drilling and hydraulic punching.

A comparative analysis of the presented results reveals that the greater the geo-stress acting on the coal seam, the

faster the gas pressure drops. When the CGO lasted for 1.84 s, the area where the test gas pressure under a geo-stress value of 4.0 MPa fell to zero was the widest. The same conclusion can be drawn from the nephogram with a time of 0.24 s. The gas pressure starts to drop from the center of the coal seam and then spreads around the coal seam. When the gas pressure in the same section is similar, the pressure drop zone will continue to extend to the coal seam. This shows that in the process of CGO, the coal body first breaks in a direction parallel to the work face, thereby generating a large number of cracks, so that the flow capacity of the gas is drastically increased. In the direction of the vertical work face, the damage to the coal body is delayed, which is related to the stress state after the formation of CGO cavern. In addition, a noteworthy phenomenon is that when the

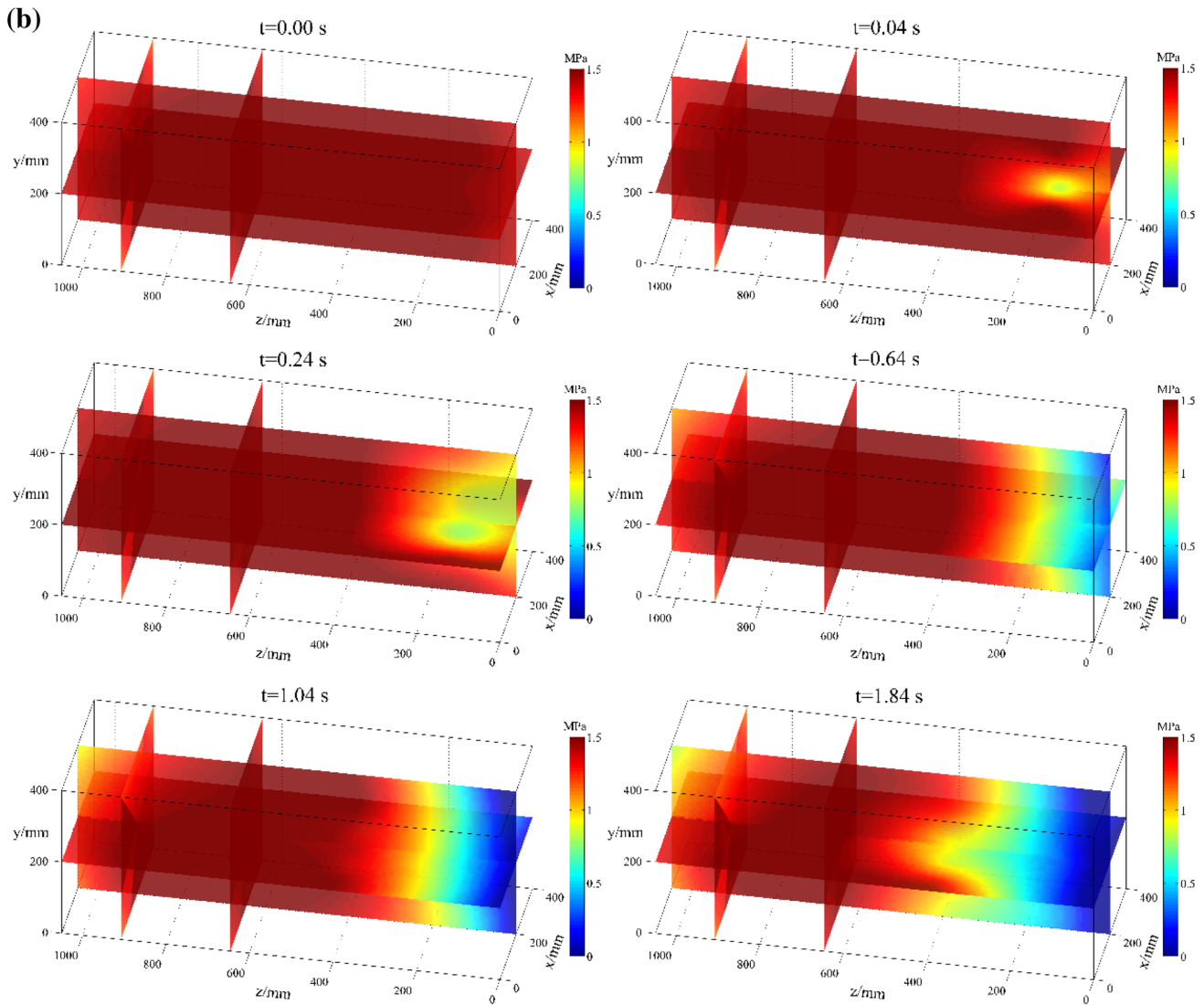


Fig. 12 (continued)

geo-stress is 1.0 MPa, the asymmetry in the gas pressure change is most obvious. This may be because a lower stress will result in more loose coal particles, making the gas flow irregularity in the coal body more random. A more in-depth analysis is required.

4 Discussion

4.1 Effects of Geological Structure and Geo-stress on CGO

As shown in Fig. 13a, the geo-stress is accumulated in the hinge zone of the fold under long-term geological extrusion. It is stored in coal seams and rock formations in the form of elastic potential energy. In particular, in the hinge zone

of the syncline structure, the upper part of the coal seam is subjected to a high static pressure of the overburden, and the lower part is subjected to the resistance of the stratum; this further squeezes the coal seam to form a relatively closed system. This geological formation not only increases the elastic potential within the coal seam, but also increases the gas pressure. When the geo-stress in the rock formations reaches a certain strength, the rock layer will break, and the accumulated elastic potential energy will be released. The fractured rock formation forms a fault structure, as shown in Fig. 13b, during subsequent crustal movement. The elastic energy is released to a certain extent because of the faults, but at the same time, a pinch-out phenomenon of the coal seam is observed. The geo-stress is significantly concentrated in the large fractures at the pinch out of the coal seam. Generally, the greater the variation in the thickness of the

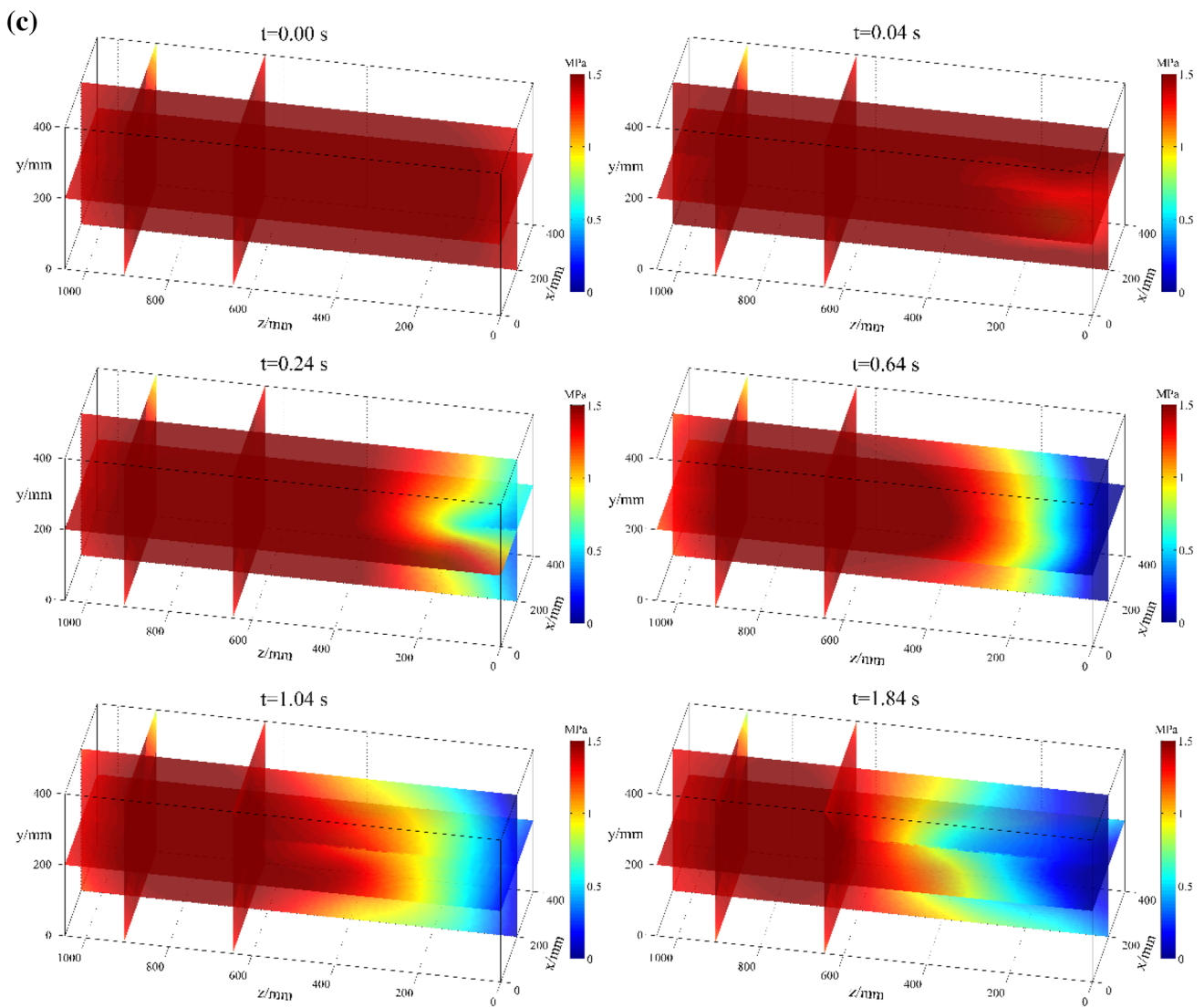
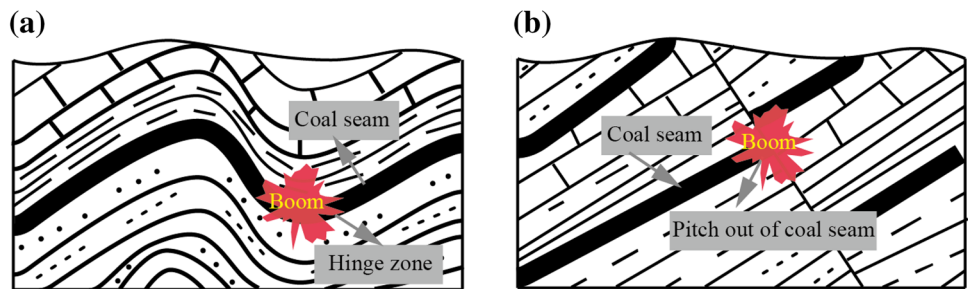


Fig. 12 (continued)

Fig. 13 Schematic of mechanical evolution during CGO



seam, the greater the stresses generated in that area (Álvarez-Fernández et al. 2009).

Furthermore, in terms of the coal quality characteristics of the area, the coal bodies in the faults and folds have a long-term geological effect, often exhibiting granular and

mylonitic features, so-called “outburst coal” (Cao et al. 2003). This coal is characterized by low strength, low permeability, and high stress sensitivity, which are also the dominant factors for CGO. When the mining or excavation face advances to the hinge of the syncline or the large

fracture at the junction of the fault and coal seam, the accumulated elastic potential is quickly released. Inside the coal seam, the energy is released in the form of stress waves. For the excavation side of the roadway, if the energy is enough to break the coal barrier in the front relief stress zone, large broken coal particles will be dumped. If there is no gas participation in the process, this dynamic phenomenon is the so-called rock burst. If there is a certain gas effect, CGO will be triggered.

In summary, both the fold structure and the fault structure increase the geo-stress and the elastic strain energy in the coal seam. In addition, this structural stress simultaneously changes the properties of the coal body and the conditions under which the gas is present. The combined effect of these factors often leads to CGO in geological structural belts.

4.2 Energy Dissipation Process Under Different Geo-stresses

In the preparation stage of CGO, the energy inputted to the coal seam mainly includes two parts: elastic strain energy and gas expansion energy. As the geo-stress value increases, the elastic strain energy gradually increases. Furthermore, the energy dissipation in the CGO process mainly includes the energy required to break the coal units and the kinetic energy of the CGO coal separating the working face (Hodot 1966; Valliappan and Zhang 1999; Jin et al. 2018; Sun et al. 2018). Obviously, an increase in the stress will result in more broken coal particles and higher initial velocity of the crushed coal during CGO. Based on a statistical analysis

conducted on a coal mine in Chongqing, China, with data from the past 30 years, Guo et al. (2010) determined the common shapes of CGO holes, as shown in Fig. 14.

In most cases, the size of the coal seam is much greater than the CGO mouth and roadway. Therefore, the CGO pulverized coal flow path can be simplified to the structure shown in Fig. 15. On the one hand, the geo-stress makes the coal mass more vulnerable, thus forming more coal particles in the process of CGO. When a large amount of pulverized coal flows through the CGO mouth, obvious choking phenomenon occurs, and at the same time, the more the pulverized coal, the more likely the occurrence of this phenomenon. On the other hand, if the outburst coal with a high solid–gas ratio is regarded as a pseudo-fluid when flowing through the structure, shown in Fig. 15, the flow velocity will increase due to the contraction of the section until the

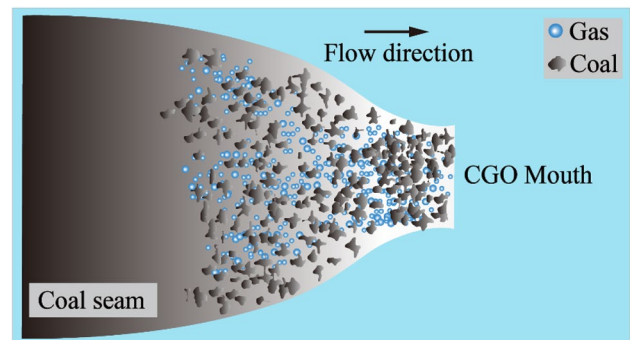


Fig. 15 Schematic of mechanical evolution during CGO

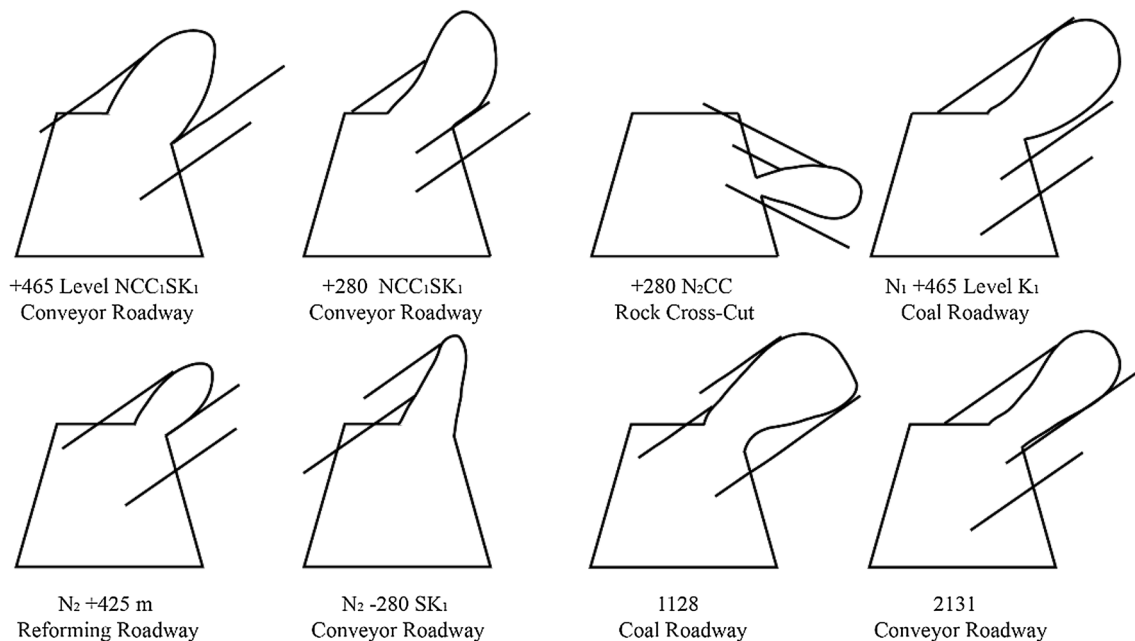


Fig. 14 Common shapes of CGO holes in a coal mine

critical sound velocity is reached. A higher geo-stress will cause coal particles to exhibit greater initial velocities, making it easier to reach the critical speed of sound. This is another reason for the choking of the two-phase coal–gas flow during the CGO process.

Furthermore, the increase in the geo-stress of the CGO will lead to an increase in the pore pressure. The change in the gas expansion energy is also a cause of the difference in the dynamic phenomenon. The above-mentioned structure, which is similar to a nozzle, seems to explain some of the unexpected phenomena, such as the velocity of the coal particles, the change in the coal seam gas pressure, and the change in the geo-stress in the process of CGO. However, the CGO process remains complex, particularly with regard to the two-phase flow. In addition, we only discussed the influence of several phenomena under different stress levels on the dynamic response of CGO. In terms of the geo-stress, the lateral pressure coefficient, stress concentration factor, and horizontal stress difference coefficient will also affect this dynamic phenomenon, which can be attributed to the direction of the geo-stress. This is subject to further research.

5 Conclusions

The influence of the tectonic, geostatic, and mining-induced stresses on CGO is mainly reflected in the magnitude and direction of the stress. We developed a custom-made large-scale physical simulation test system to conduct experimental research on the dynamic response characteristics of CGO to different geo-stress levels, to overcome dynamic disasters in coal mines. We analyzed the characteristics of the motion of solid-phase pulverized coal, evolution of the geo-stress acting on the coal seam, and variations in the elastic strain energy and gas pressure in the process of CGO. The following conclusions can be drawn from the experimental research conducted:

(1) When the initial geo-stresses of the coal seam are 1.0, 2.0, and 4.0 MPa, the CGO relatively intensities are 6.35, 7.97, and 8.95%, respectively, i.e., the CGO intensity increases with increasing geo-stress. The initial velocity of the outburst coal also increases with increasing geo-stress. Releasing the stress can significantly reduce the CGO intensities, and at the same time reduce the initial kinetic energy of the coal–gas two-phase flow. However, we observed a mechanism that suppresses the excess energy released during the dynamic process, such that the solid–gas ratio of the CGO two-phase flow does not continue to increase with increasing initial geo-stress. In addition, the outburst coal exhibits intermittent vibration characteristics.

(2) The geo-stress changes during the CGO process are mainly manifested in the relief and abutment stress zones, whereas the geo-stress in the recovered and initial stress zones exhibits only slight fluctuations. Therefore, the release of stress must extend to at least the abutment stress zone. Simultaneously, the geo-stress change in the abutment stress zone lags behind that in the relief stress zone, indicating that CGO is a dynamic process from the beginning of the relief stress zone to the deep transfer of the coal body. The change in the geo-stress is not a monotonous process; it appears to fluctuate during the CGO.

(3) The release of the elastic strain energy during CGO is manifested in the abutment stress zone. This shows that effectively determining the extent of the stress concentration zone is the key to reducing the energy of CGO. The release of the strain energy during CGO process also exhibits periodic characteristics. When the initial stress of the coal seam is increased by four times from 1 MPa, the elastic strain energy released increases by more than nine times. Therefore, when the burial depth of the coal seam is high or when the structural stress increases sharply, the elastic strain energy can no longer be ignored in the analysis of CGO energy.

(4) During the process of CGO, the gas pressure decrease in the relief and abutment stress zones shows fluctuation characteristics; this is more obvious with increasing geo-stress. In addition to the relief stress zone, both the gas pressure drop rate and decrease amount during the CGO process increase with increasing geo-stress. This indicates that increase in geo-stress will significantly increase the release of gas expansion energy during the CGO process. The gas pressure starts to decrease from the center of the coal seam and then spreads around the coal seam. The gas pressure is largely released in the relief and abutment stress zones. As such, if we can determine the extent of the change in the gas pressure during this process, it would aid in setting the drilling depth in measures to eliminate CGO.

Based on the above conclusions, the following prospects can be drawn to guide the prevention and understanding of CGO in-situ: In deep coal mines, the contribution of the elastic strain energy to the CGO caused by the increased geo-stress will increase significantly. Therefore, the search for the limit equilibrium stress zone and the division of the stress distribution zone in front of the working face are essential to prevent CGO. In addition, with the increase of geo-stress, a choking phenomenon will spontaneously occur in the coal seam, which will mislead workers to feel that the CGO dynamic phenomenon is weakened, but the energy in the coal seam is not released. When the CGO

cavern increases and the choking disappears, this part of energy will still be released once again.

The present study was based on the analysis of physical simulation experimental results. Some of the findings require further verification of the field data, though this will be difficult for dynamic phenomena such as CGO. Nevertheless, this study can serve as a basis for analyzing the mechanism of geo-stress in the process of CGO.

Acknowledgements This work was supported by the National Science and Technology Major Project of China [No. 2016ZX05044002]; the National Natural Science Foundation of China [No. 51874055, 51974041]; and the China Postdoctoral Science Foundation [No. 2018M633317].

Compliance with Ethical Standards

Conflict of interest The authors declare that they have no conflict of interest.

References

- Aguado MBD, González C (2009) Influence of the stress state in a coal bump-prone deep coalbed: a case study. *Int J Rock Mech Min Sci* 46:333–345. <https://doi.org/10.1016/j.ijrmms.2008.07.005>
- Aguado MBD, Nicieza CG (2007) Control and prevention of gas outbursts in coal mines, Riosa-Olloniego coalfield, Spain *Int J Coal Geol* 69:253–266. <https://doi.org/10.1016/j.coal.2006.05.004>
- Alexeev AD, Revva VN, Alyshev NA, Zhitlyonok DM (2004) True triaxial loading apparatus and its application to coal outburst prediction. *Int J Coal Geol* 58:245–250. <https://doi.org/10.1016/j.coal.2003.09.007>
- Álvarez-Fernández MI, González-Nicieza C, Álvarez-Vigil AE, Herrera García G, Torno S (2009) Numerical modelling and analysis of the influence of local variation in the thickness of a coal seam on surrounding stresses: application to a practical case. *Int J Coal Geol* 79:157–166. <https://doi.org/10.1016/j.coal.2009.06.008>
- An FH, Yuan Y, Chen XJ, Li ZQ, Li LY (2019) Expansion energy of coal gas for the initiation of coal and gas outbursts. *Fuel* 235:551–557. <https://doi.org/10.1016/j.fuel.2018.07.132>
- Cai MF (2002) *Rock mechanics and engineering*. Science Press, Beijing
- Cao YX, Davis A, Liu RX, Liu XW, Zhang YG (2003) The influence of tectonic deformation on some geochemical properties of coals—a possible indicator of outburst potential. *Int J Coal Geol* 53:69–79. [https://doi.org/10.1016/S0166-5162\(02\)00077-0](https://doi.org/10.1016/S0166-5162(02)00077-0)
- Cao J, Sun HT, Wang B, Dai LC, Zhao B, Wen GC, Zhao XS (2019) A novel large-scale three-dimensional apparatus to study mechanisms of coal and gas outburst. *Int J Rock Mech Min Sci* 118:52–62. <https://doi.org/10.1016/j.ijrmms.2019.04.002>
- Chen KP (2011) A new mechanistic model for prediction of instantaneous coal outbursts—dedicated to the memory of Prof. Daniel D. Joseph. *Int J Coal Geol* 87:72–79. <https://doi.org/10.1016/j.coal.2011.04.012>
- Ding YL, Yue ZQ (2018) An experimental investigation of the roles of water content and gas decompression rate for outburst in coal briquettes. *Fuel* 234:1221–1228. <https://doi.org/10.1016/j.fuel.2018.07.143>
- Dutka B, Kudasik M, Pokryszka Z, Skoczylas N, Topolnicki J, Wierzbicki M (2013) Balance of CO₂/CH₄ exchange sorption in a coal briquette. *Fuel Process Technol* 106:95–101. <https://doi.org/10.1016/j.fuproc.2012.06.029>
- Geng J, Xu J, Nie W, Peng S, Zhang C, Luo X (2017) Regression analysis of major parameters affecting the intensity of coal and gas outbursts in laboratory. *Int J Min Sci Technol* 27:327–332. <https://doi.org/10.1016/j.ijmst.2017.01.004>
- Guo CY, Xian XF, Yao WJ, Jiang YD (2010) Relationship between the fracture zone and cave of coal or gas outburst caving in coal and rock seams. *J China U Min T* 36:802–807. [https://doi.org/10.1016/S1876-3804\(11\)60004-9](https://doi.org/10.1016/S1876-3804(11)60004-9)
- Hashemi SS, Melkounian N (2016) A strain energy criterion based on grain dislodgment at borehole wall in poorly cemented sands. *Int J Rock Mech Min Sci* 87:90–103. <https://doi.org/10.1016/j.ijrmms.2016.05.013>
- Hodot BB (1966) *Outburst of coal and coalbed gas*. China Industry Press, Beijing
- Huang D, Li Y (2014) Conversion of strain energy in triaxial unloading tests on marble. *Int J Rock Mech Min Sci* 66:160–168. <https://doi.org/10.1016/j.ijrmms.2013.12.001>
- International Energy Agency (2019) *Coal information 2019*. Organisation for Economic Co-operation and Development, Paris
- Jasinge D, Ranjith PG, Choi SK (2011) Effects of effective stress changes on permeability of Latrobe valley brown coal. *Fuel* 90:1292–1300. <https://doi.org/10.1016/j.fuel.2010.10.053>
- Jaworski AJ, Dyakowski T (2002) Investigations of flow instabilities within the dense pneumatic conveying system. *Powder Technol* 125:279–291. [https://doi.org/10.1016/S0032-5910\(01\)00516-2](https://doi.org/10.1016/S0032-5910(01)00516-2)
- Jiang JY, Cheng YP, Wang L, Li W, Wang L (2011) Petrographic and geochemical effects of sill intrusions on coal and their implications for gas outbursts in the Wolonghu Mine, Huaibei Coalfield, China. *Int J Coal Geol* 88:55–66. <https://doi.org/10.1016/j.coal.2011.08.007>
- Jin K, Cheng YP, Ren T, Zhao W, Tu QY, Dong J, Wang ZY, Hu B (2018) Experimental investigation on the formation and transport mechanism of outburst coal-gas flow: implications for the role of gas desorption in the development stage of outburst. *Int J Coal Geol* 194:45–58. <https://doi.org/10.1016/j.coal.2018.05.012>
- Lama RD, Bodziony J (1998) Management of outburst in underground coal mines. *Int J Coal Geol* 35:83–115. [https://doi.org/10.1016/S0166-5162\(97\)00037-2](https://doi.org/10.1016/S0166-5162(97)00037-2)
- Li H (2001) Major and minor structural features of a bedding shear zone along a coal seam and related gas outburst, Pingdingshan coalfield, northern China. *Int J Coal Geol* 47:101–113. [https://doi.org/10.1016/S0140-6701\(02\)86160-4](https://doi.org/10.1016/S0140-6701(02)86160-4)
- Li H, Feng ZC, Zhao D, Duan D (2017) Simulation experiment and acoustic emission study on coal and gas outburst. *Rock Mech Rock Eng* 50:2193–2205. <https://doi.org/10.1007/s00603-017-1221-3>
- Li SC, Li QC, Wang HP, Yuan L, Zhang YQ, Xue JH, Zhang B, Wang J (2018) A large-scale three-dimensional coal and gas outburst quantitative physical modeling system. *J China Coal Soc* 43(S1):121–129. <https://doi.org/10.13225/j.cnki.jccs.2017.1076>
- Liu YB, Yin GZ, Li MH, Zhang DM, Deng BZ, Liu C, Lu J (2019) Anisotropic mechanical properties and the permeability evolution of cubic coal under true triaxial stress paths. *Rock Mech Rock Eng* 52:2505–2521. <https://doi.org/10.1007/s00603-019-01748-1>
- Lu YY, Wang HY, Xia BW, Li XH, Ge ZL, Tang JR (2017) Development of a multi-functional physical model testing system for deep coal petrography engineering. *Rock Mech Rock Eng* 50:269–283. <https://doi.org/10.1007/s00603-016-1124-8>
- Nie BS, Ma YK, Meng JQ, Hu ST (2015) Middle scale simulation system of coal and gas outburst. *Chin J Rock Mech Eng* 37:1218–1225. <https://doi.org/10.13722/j.cnki.jrme.2017.1125>
- Peng RD, Ju Y, Wang JG, Xie HP, Gao F, Mao LT (2015) Energy dissipation and release during coal failure under conventional triaxial compression. *Rock Mech Rock Eng* 48:509–526. <https://doi.org/10.1007/s00603-014-0602-0>

- Qian XS (1966) Gas dynamics equations. Science, Beijing
- Sandwell DT (1987) Biharmonic spline interpolation of GEOS-3 and SEASAT altimeter data. *Geophys Res Let* 14:139–142. <https://doi.org/10.1029/GL014i002p00139>
- Shankar PN, Deshpande MD (2003) Fluid mechanics in the driven cavity. *Annu Rev Fluid Mech* 32:93–136. <https://doi.org/10.1146/annurev.fluid.32.1.93>
- Shapiro AH (1953) The dynamics and thermodynamics of compressible fluid flow. Ronald, New York
- Singh JG (1984) A mechanism of outbursts of coal and gas. *Min Sci T* 1:269–273. [https://doi.org/10.1016/S0167-9031\(84\)90309-8](https://doi.org/10.1016/S0167-9031(84)90309-8)
- Skoczylas N, Wierzbicki M (2014) Evaluation and management of the gas and rock outburst hazard in the light of international legal regulations. *Arch Min Sci* 59:1119–1129. <https://doi.org/10.2478/amsc-2014-0078>
- Skoczylas N, Dutka B, Sobczyk J (2014) Mechanical and gaseous properties of coal briquettes in terms of outburst risk. *Fuel* 134:45–52. <https://doi.org/10.1016/j.fuel.2014.05.037>
- Sobczyk J (2011) The influence of sorption processes on gas stresses leading to the coal and gas outburst in the laboratory conditions. *Fuel* 90:1018–1023. <https://doi.org/10.1016/j.fuel.2010.11.004>
- Su XP (2014) Molding condition optimization of coal containing gas and its application in physical simulation of CBM extraction. Chongqing University, Chongqing
- Sun Q, Zhang JX, Zhang Q, Yin W, Germain D (2016) A protective seam with nearly whole rock mining technology for controlling coal and gas outburst hazards: a case study. *Nat Hazards* 84:1793–1806. <https://doi.org/10.1007/s11069-016-2512-9>
- Sun HT, Cao J, Li MH, Zhao XS, Dai LC, Sun DL, Wang B, Zhai BN (2018) Experimental research on the impactive dynamic effect of gas-pulverized coal of coal and gas outburst. *Energies* 11:797. <https://doi.org/10.3390/en11040797>
- Tu QY, Cheng YP, Guo PK, Jiang JY, Wang L, Zhang R (2016) Experimental study of coal and gas outbursts related to gas-enriched areas. *Rock Mech Rock Eng* 49:3769–3781. <https://doi.org/10.1007/s00603-016-0980-6>
- Valliappan S, Zhang WH (1999) Role of gas energy during coal outbursts. *Int J Numer Meth Eng* 44:875–895. [https://doi.org/10.1002/\(SICI\)1097-0207\(19990310\)44:73.0.CO;2-G](https://doi.org/10.1002/(SICI)1097-0207(19990310)44:73.0.CO;2-G)
- Wang CJ, Yang SQ, Li JH, Li XW, Jiang CL (2018a) Influence of coal moisture on initial gas desorption and gas-release energy characteristics. *Fuel* 232:351–361. <https://doi.org/10.1016/j.fuel.2018.06.006>
- Wang CJ, Yang SQ, Li XW, Yang DD, Jiang CL (2018b) The correlation between dynamic phenomena of boreholes for outburst prediction and outburst risks during coal roadways driving. *Fuel* 231:307–316. <https://doi.org/10.1016/j.fuel.2018.05.109>
- Wang CJ, Yang SQ, Yang DD, Li XW, Jiang CL (2018c) Experimental analysis of the intensity and evolution of coal and gas outbursts. *Fuel* 226:252–262. <https://doi.org/10.1016/j.fuel.2018.03.165>
- Wold MB, Connell LD, Choi SK (2008) The role of spatial variability in coal seam parameters on gas outburst behaviour during coal mining. *Int J Coal Geol* 75:1–14. <https://doi.org/10.1016/j.coal.2008.01.006>
- Xie GX, Yin ZQ, Wang L, Hu ZX, Zhu CQ (2017) Effects of gas pressure on the failure characteristics of coal. *Rock Mech Rock Eng* 50:1711–1723. <https://doi.org/10.1007/s00603-017-1194-2>
- Xie HP, Gao MZ, Zhang R, Peng GY, Wang WY, Li AQ (2019) Study on the mechanical properties and mechanical response of coal mining at 1000 m or deeper. *Rock Mech Rock Eng* 52:1475–1490. <https://doi.org/10.1007/s00603-018-1509-y>
- Xue S, Yuan L, Wang YC, Xie J (2014) Numerical analyses of the major parameters affecting the initiation of outbursts of coal and gas. *Rock Mech Rock Eng* 47:1505–1510. <https://doi.org/10.1007/s00603-013-0425-4>
- Yin GZ, Li MH, Wang JG, Xu J, Li WP (2015) Mechanical behavior and permeability evolution of gas infiltrated coals during protective layer mining. *Int J Rock Mech Min Sci* 80:292–301. <https://doi.org/10.1016/j.ijrmms.2015.08.022>
- Zhang QH, Yuan L, Wang HP, Kang JH, Li SC, Xue JH, Zhou W, Zhang DM (2016) Establishment and analysis of similarity criteria for physical simulation of coal and gas outburst. *J China Coal Soc* 41:2773–2779
- Zhang CL, Xu J, Peng SJ, Zhang XL, Liu XR, Chen YX (2018) Dynamic evolution of coal reservoir parameters in CBM extraction by parallel boreholes along coal seam. *Transport Porous Med* 124:1–19. <https://doi.org/10.1007/s11242-018-1067-5>
- Zhao W, Cheng YP, Jiang HN, Jin K, Wang HF, Wang L (2016) Role of the rapid gas desorption of coal powders in the development stage of outbursts. *J Nat Gas Sci Eng* 28:491–501. <https://doi.org/10.1016/j.jngse.2015.12.025>
- Zhao W, Cheng YP, Guo PK, Jin K, Tu QY, Wang HF (2017) An analysis of the gas-solid plug flow formation: new insights into the coal failure process during coal and gas outbursts. *Powder Technol* 305:39–47. <https://doi.org/10.1016/j.powtec.2016.09.047>
- Zhao B, Wen GC, Sun HT, Yang HM, Cao J, Dai LC, Wang B (2018) Similarity criteria and coal-like material in coal and gas outburst physical simulation. *Int J Coal Sci T* 5:167–178. <https://doi.org/10.1007/s40789-018-0203-8>
- Zhou HX, Gao J, Han K, Cheng YP (2018) Permeability enhancements of borehole outburst cavitation in outburst-prone coal seams. *Int J Rock Mech Min Sci* 111:12–20. <https://doi.org/10.1016/j.ijrmms.2018.07.008>
- Zhou B, Xu J, Peng S, Yan FZ, Yang W, Cheng L, Ni GH (2019) Experimental analysis of the dynamic effects of coal-gas outburst and a protean contraction and expansion flow model. *Nat Resour Res*. <https://doi.org/10.1007/s11053-019-09552-y>

Publisher's Note Springer Nature remains neutral with regard to jurisdictional claims in published maps and institutional affiliations.